Bone 122 (2019) 114–122

Contents lists available at ScienceDirect

Bone

journal homepage: www.elsevier.com/locate/bone

Full Length Article

Treatment with an inhibitor of fatty acid synthase attenuates bone loss in ovariectomized mice

Sandra Bermeo[a,b], Ahmed Al Saedi[c,d], Christopher Vidal[a], Mamdouh Khalil[e], Manhui Pang[f], Bruce R. Troen[f], Damian Myers[c,d], Gustavo Duque[a,c,d,*]

[a] Sydney Medical School Nepean, The University of Sydney, Penrith, NSW 2750, Australia
[b] Facultad de Ciencias Básicas y Biomédicas, Universidad Simón Bolívar, Barranquilla, Colombia
[c] Australian Institute for Musculoskeletal Science (AIMSS), The University of Melbourne and Western Health, St Albans, VIC 3021, Australia
[d] Department of Medicine-Western Health, Melbourne Medical School, The University of Melbourne, St Albans, VIC 3021, Australia
[e] ANZAC Research Institute, Sydney Medical School Concord, The University of Sydney, Concord, NSW 2137, Australia
[f] Division of Geriatrics and Palliative Medicine, Jacobs School of Medicine and Biomedical Sciences and Research Service, Veterans Affairs Western New York Healthcare System, University at Buffalo, Buffalo, NY, USA

ARTICLE INFO

Keywords:
Cerulenin
Fatty acid synthase
Adipogenesis
Osteoblastogenesis
Osteoporosis

ABSTRACT

Bone and fat cells have an antagonistic relationship. Adipocytes exert a toxic effect on bone cells *in vitro* through the secretion of fatty acids, which are synthesized by fatty acid synthase (FAS). Inhibition of FAS *in vitro* rescues osteoblasts from fat-induced toxicity and cell death. In this study, we hypothesized that FAS inhibition would mitigate the loss of bone mass in ovariectomized (OVX) mice. We treated OVX C57BL/6 mice with cerulenin (a known inhibitor of FAS) for 6 weeks and compared their bone phenotype with vehicle-treated controls. Cerulenin-treated mice exhibited a significant decrease in body weight, triglycerides, leptin, and marrow and subcutaneous fat without changes in serum glucose or calciotropic hormones. These effects were associated with attenuation of bone loss and normalization of the bone phenotype in the cerulenin-treated OVX group compared to the vehicle-treated OVX group. Our results demonstrate that inhibition of FAS enhances bone formation, induces uncoupling between osteoblasts and osteoclasts, and favors mineralization, thus providing evidence that inhibition of FAS could constitute a new anabolic therapy for osteoporosis.

1. Introduction

The traditional understanding of the mechanisms of osteoporosis has been based on either high levels of bone resorption by the osteoclasts or low levels of bone formation by the osteoblasts [1]. In the same direction, antiresorptives, such as bisphosphonates, or anabolics, such as teriparatide, have been the predominant therapeutic approach to osteoporosis for the last two decades [1]. However, the effectiveness of these medications may have reached a plateau while side effects such as osteonecrosis of the jaw and atypical fractures have been reported [2]. Therefore, new approaches to the treatment of osteoporosis are still desirable.

The progressive marrow fat infiltration observed both in osteoporosis and aging is now considered as the “obesity of bone” [3]. High levels of marrow fat have been associated with either decreased osteoblast differentiation and bone formation or increased levels of bone resorption by the osteoclasts [4]. In addition, marrow adipocytes exert a toxic effect on differentiated osteoblasts [4–7], a process known as lipotoxicity.

Lipotoxicity, defined in Stedman's Medical Dictionary as the “pathologic changes in organs resultant from elevated fat levels in blood or tissues, as in the diabetic liver” [8], has been associated with metabolic disorders such as diabetes, hypertension, atherosclerosis, and metabolic syndrome by interacting and amplifying the effect of other mechanisms such as inflammation [9]. Lipotoxicity is also considered one of the mechanisms that aggravate age-related bone loss following the progressive accumulation of marrow fat and the secretion of fatty acids and adipokines within the bone marrow milieu [4].

In addition to the lipotoxic effect of marrow adipocytes on osteoblasts [5–7], increasing levels of marrow fat have an indirect effect on bone resorption by stimulating osteoclast function [10,11]. In fact, it has been reported that factors produced by adipocytes in culture

* Corresponding author at: Australian Institute for Musculoskeletal Science (AIMSS), The University of Melbourne and Western Health, 176 Furlong Road, St Albans, VIC 3021, Australia.
E-mail address: gustavo.duque@unimelb.edu.au (G. Duque).

https://doi.org/10.1016/j.bone.2019.02.017
Received 6 November 2018; Received in revised form 3 February 2019; Accepted 15 February 2019
Available online 16 February 2019

promote osteoclast differentiation [11], resulting in an altered bone turnover with enhanced bone resorption and subsequent bone loss [12].

This lipotoxic effect of marrow fat is not common to all regions of the bone and is clearly context- and location-dependent. However, the areas of the bones that are predominantly affected by osteoporosis, such as proximal femur and lumbar spine, also show progressively high levels of fat infiltration, which are significantly higher in osteoporosis [3], thus suggesting a deleterious role of fat on bone mass and quality in those anatomical sites.

Although understanding the mechanisms underlying the fat and bone relationship is of major interest, the potential therapeutic implications of regulating this relationship to increase bone mass and treat osteoporosis remain unexplored [13]. Potential strategies could consist of either returning the osteoblast/adipocyte ratio to normal levels, or stimulating osteoblast differentiation and function at the expense of the number of differentiated adipocytes and the regulation of their secreted factors. These two alternatives are supported by the fact that adipocytes and osteoblasts share their mesenchymal origin and co-habit in the same lipotoxic bone marrow milieu [14].

We have previously reported the deleterious effect that adipocyte-secreted fatty acids have on human osteoblasts survival and function *in vitro* [5–7]. Interestingly, the lipotoxic effect of adipocytes on osteoblasts *in vitro* was prevented by the inhibition of fatty acid synthase (FAS) after adding cerulenin into the media. Cerulenin [(2S, 3R)-2,3-epoxy-4-oxo-7,10-dodecadienoylamide] is an intestine-absorbed natural antibiotic that inhibits the *de novo* synthesis of fatty acids (mainly palmitate) by blocking β-ketoacyl synthase, one of the seven domains of the FAS complex [15,16], and to a lesser extent Acetyl-CoA carboxylase. As an additional mechanism of action, cerulenin blocks the endogenous production of fatty acids *via* sterol regulatory element-binding protein-1 (SREBP-1), thus limiting the increased lipogenesis that is commonly observed in aging organs and tissues [17].

In this study, we hypothesized that treatment *in vivo* with cerulenin would protect osteoblasts from lipotoxicity while rescuing oophorectomized mice (OVX) from their osteoporotic phenotype. Our objective was to investigate an innovative approach to bone formation in osteoporotic animals, which could be translated into human studies in the future.

2. Materials and methods

2.1. Animals

We purchased 9-month-old C57BL/6 mice (n = 10 per group) from The Animal Resources Centre (Canning Vale, WA, Australia). Bilateral OVX was performed under general anesthesia. Another group of animals was sham-operated (SHAM) in which ovaries were exteriorized but replaced intact. Six weeks after surgery, cerulenin (Sigma, St. Louis, MO, USA) was prepared by solubilizing in ethanol 100%, diluted 1:5 in RPMI 1640 medium (GIBCO®, Life technologies Pty Ltd., Australia), and administered subcutaneously to the OVX mice at a concentration of 30 mg/kg body weight or vehicle (RPMI 1640) at days 1, 4 and 7 per 6 weeks (Fig. 1A). Mice were housed in cages in a limited access room located at the ANZAC Research Institute (Sydney, Australia). The Sydney South West Area Health Service (SSWAHS) animal welfare committee approved animal husbandry and protocols.

2.2. Ex vivo cultures and staining

Tibiae from vehicle-treated SHAM (SHAM), vehicle-treated OVX (VEH-OVX) and cerulenin-treated OVX (CER-OVX) groups (n = 10 per group) were flushed using a 21-gauge needle attached to a 10 ml syringe filled with Dulbecco's modified Eagle's Medium (DMEM) (GIBCO BRL, Gaithersburg, MD, USA). Cells from both tibiae were filtered through a cell strainer with 70-μm nylon mesh (BD Bioscience, Bedford, MA, USA) and then combined to produce a volume of 2 ml containing ~10^7 cells/ml. Cultures were then established in triplicate in 6-well plates, with each well containing a 100-μl aliquot of cell suspension combined with 4 ml of fresh α-MEM medium. Cells were incubated in mesenchymal stem cell growth media (MSCGM) at 37 °C with 5% humidified CO_2 and isolated by their adherence to tissue culture plastic. Medium was aspirated and replaced with fresh medium every 2 to 3 days to remove non-adherent cells. The adherent cells were grown to ~80% confluence for about 7 days defined as bone marrow stromal cells (BMSC) at passage 0, harvested with 0.25% trypsin and 1 mM EDTA for 5 min at 37 °C, diluted 1:3 in MSCGM, plated and grown to confluence for further expansion. After 2nd and 3rd passages, BMSC were used for subsequent experiments.

To induce osteogenic differentiation, a total of 10^4 cells were diluted in osteogenic medium (prepared with DMEM, 10% FCS, 0.2 mM dexamethasone, 10 mmol/L β glycerol phosphate and 50 μg/ml ascorbic acid) and plated in 6-well plates. Media was aspirated and replaced with fresh osteogenic medium every 3 days. After 14 days in culture, cells were washed with PBS, ethanol fixed and stained for alkaline phosphatase using the 86R staining system (Sigma, St. Louis, MO, USA) according to the manufacturer's instructions.

For adipocyte differentiation, cells were obtained and plated as previously described [19]. After passage 3, 10^4 BMSC were diluted in adipogenic medium (prepared with DMEM, 4.5 g/L glucose, 1 μM dexamethasone, 0.2 mM indomethacin, 1.7 μM insulin, 0.5 mM 3-isobutyl-1-methylxanthine, 10% FCS, 0.05 U/ml penicillin, and 0.05 μg/ml streptomycin) and plated in 6-well plates for 3 days. To promote the adipogenic phenotype, cells were then incubated for 3 days in adipogenesis maintenance medium (DMEM, 4.5 g/L glucose, 1.7 μM insulin, 10% FBS, 0.05 U/ml penicillin, and 0.05 μg/ml streptomycin) and then switched to induction media again. After 3 cycles of induction/maintenance (day 18), media was aspirated, and cells were fixed, and adipocytes visualized by staining with Oil Red O (ORO). Cells were then washed 4 times with running tap water to remove excess stain. ORO was eluted with 1 ml 100% isopropanol for 10 min and absorbance measured at 490 nm. For quantification of mineralization, Alizarin red was quantified by spectrophotometry after adding 10% cetylpyridinium chloride (CPC) in 10 mM sodium phosphate pH 7.0 to the media for 15 min at room temperature to de-stain and then measuring absorbance at 562 nm.

ORO, Alkaline Phosphatase and Alizarin Red values were corrected against cell density, which was determined by DAPI (4,6-diamidino-2-phenylindole) staining. To quantify adipocyte number, two independent observers counted the number of ORO stained cells in 10 fields per well in 6 replicates wells per group. All photomicrographs were taken using an IX50 Olympus inverted microscope (Olympus®, Tokyo, Japan) and a Digital Sight DS-5M Nikon camera (Nikon Instruments, Inc. Melville, New York, USA).

2.3. RT-PCR and Western Blot

Both humeri were flushed as previously described. Bone marrow cell RNA and proteins were obtained using the PARIS™ protocol (Ambion Inc., Austin, TX, USA) according to the protocol instructions in the presence of Halt™ protease and phosphatase inhibitors (Thermo Fisher Scientific Inc. Rockford, IL, USA). Protein concentration was measured using the BCA Protein Assay Reagent kit (Thermo Fisher Scientific Inc. Rockford, IL USA). RNA concentrations and purity were estimated based on UV absorbance readings by spectrophotometry at 260 nm. First strand complementary DNA (cDNA) synthesis was performed using 200 ng of total RNA, 50 ng random hexamers and 50 units reverse transcriptase at 42 °C for 1 h, as described by manufacturer (Bioline Australia Pty, Alexandria, NSW, Australia; cat# BIO-65025). Real-time PCR for expressed genes as markers for osteogenesis/adipogenesis was performed in duplicate in a total reaction volume of 25 μl, 10% of which was cDNA (or water for non-template control), 3 mM $MgCl_2$ and 250 nM of each forward and reverse specific primer for

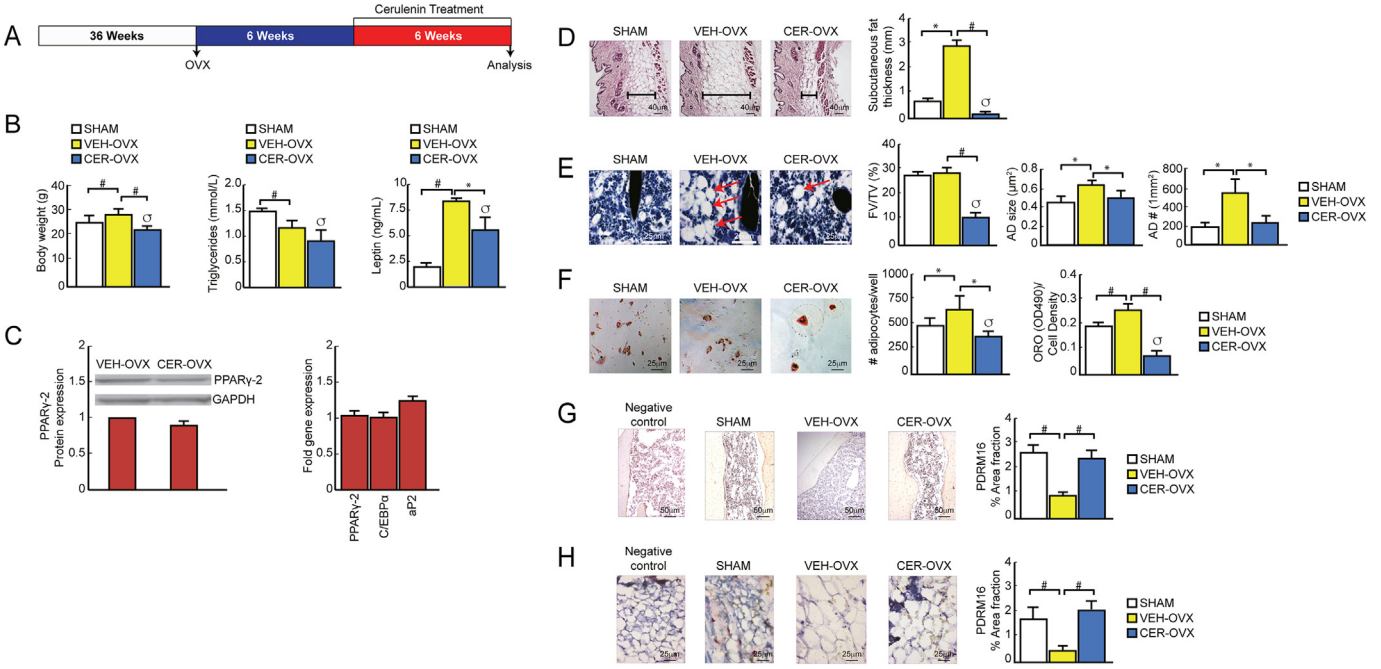

Fig. 1. Effect of FAS inhibition on bone marrow fat content and adipogenesis. Nine-month old C57BL/6 male mice ($n = 10$ per group) were treated with cerulenin or vehicle as described in Materials and methods. (A) Timeline of ovariectomy, cerulenin treatment and analysis. (B) Effect of cerulenin on body weight, serum triglycerides and leptin. $*p < 0.001$ (C) Effect of FAS inhibition on protein and gene expression of selected adipogenic factors in bone marrow obtained from CER-OVX mice as compared with VEH-OVX animals; all values were corrected with GAPDH. (D) FAS inhibition induced a decrease in subcutaneous fat thickness in CER-OVX mice (magnification 10×). (E) Fat content in bone marrow (left panels, red arrows, magnification 25×) stained with von Kossa expressed as percentage of fat volume/total volume FV/TV and adipocyte parameters: size and number, were measured. (F) *Ex vivo* adipogenesis after three weeks in differentiation media expressed as the number of adipocytes per well quantified by two independent investigators. Lipid accumulation was determined by ORO quantification (OD 490) and values corrected against cell density. Values are mean ± SD, $*p < 0.05$, $\#p < 0.001$, $\sigma p < 0.05$ between the SHAM and the VEH-OVX and CER-OVX groups. (G) IHC of bone marrow sections from tibiae for PRDM16 (marker of brown adipose tissue). Values are mean ± SD, $\#p < 0.001$ (magnification 10×) (H) IHC of subcutaneous sections for PRDM16 (brown fat marker). Values are mean ± SD, $\#p < 0.001$ (magnification 25×). (For interpretation of the references to colour in this figure legend, the reader is referred to the web version of this article.)

Table 1
Sequence of primers used for RT-PCR analysis. Forward and reverse sequences are in 5′ to 3′ direction. PPARγ: Peroxisome proliferator activator gamma; C/EBPα: CCAAT/enhancer binding protein alpha; aP2: Adipocyte protein 2; RANKL: Receptor activator of nuclear factor kappa-B ligand; RUNX2: Runt-related transcription factor 2; OCN: Osteocalcin; OPN: Osteopontin; BSP: Bone sialoprotein; GAPDH: Glyceraldehyde 3-phosphate dehydrogenase.

Primer name	Forward	Reverse
PPARγ	TCACAAGAGCTGACCCAATGG	GATCGCACTTTGGTATTCTTGGA
C/EBPα	GAGCTGAGTGAGGCTCTCATTCT	TGGGAGGCAGACGAAAAAAC
aP2	GCGTGGAATTCGATGAAATCA	CCCGCCATCTAGGGTTATGA
RANKL	AGCCGAGACTACGGCAAGTA	GCGCTCGAAAGTACAGGAAC
RUNX2	GCCGGGAATGATGAGAACTA	GGACCGTCCACTGTCACTTT
OCN	CTTGGTGCACACCTAGCAGA	ACCTTATTGCCCTCCTGCTT
OPN	TGCACCCAGATCCTATAGCC	CTCCATCGTCATCATCATCG
BSP	AAAGTGAAGGAAAGCGACGA	GTTCCTTCTGCACCTGCTTC
GAPDH	AACTTTGGCATTGTGGAAGG	ACACATTGGGGGTAGGAACA

target genes and normalizer (Table 1). All PCRs were performed in a Corbett Rotor-Gene™ 3000 (QIAGEN Pty) using SYBR green with no-ROX reaction mix and a standard thermal profile as described by supplier (Bioline Australia Pty, Alexandria, NSW, Australia; cat# QT650-02). Quantitative RT-PCR data was defined by threshold cycle (Ct) normalized for the housekeeping gene glyceraldehyde-3-phosphate dehydrogenase (GAPDH). Quantification of relative differences of expressed genes between the three conditions were calculated using REST software (QIAGEN Pty) [19] correcting for PCR reaction efficiencies (> 0.90).

Proteins were reduced with DTT 50 mM in NuPAGE® LDS Sample Buffer 1× (Invitrogen Corporation, Carlsbad, CA, USA), separated by SDS-PAGE 4–12% 90 min at 120 V and transferred to a 0.2 μm PVDF membrane (Bio-Rad Laboratories, Inc., Hercules, CA, USA) 50 min at 150 mA. After blocking with BSA 5% for 1 h, membranes were incubated with primary antibodies adiponectin (MA1-054, Thermo Fisher Scientific Inc. Rockford, IL, USA), PPARγ-2, Runt-related transcription factor 2 (RUNX2), osteopontin (OPN) (Sc-22020-R, Sc-12488, Sc-21742 respectively; Santa Cruz Biotechnology Inc. Santa Cruz, CA, USA), osteocalcin (OCN) (250483, Abbiotec LLC, San Diego, CA, USA) and bone sialoprotein (BSP) (Abbiotec LLC, San Diego, CA, USA) overnight at 4 °C. After three washes with 1× TBS (20 mM Tris base and 0.15 M NaCl) + 0.5% tween 20 buffer, the membranes were incubated for 1 h at room temperature with secondary antibody conjugated with horseradish peroxidase (HRP). Immunoblots were analyzed by enhanced chemiluminescence (Thermo Fisher Scientific Inc. Rockford, IL, USA) using the Quantity One 4.4.0 software (Bio-Rad Laboratories, Hercules, CA, USA). Blot intensities were quantified using ImageJ software.

2.4. μ-CT analysis

Structural analysis of the bone was performed using micro computed tomography (μ-CT) in the left femur after removal of soft tissues and overnight fixation in 4% paraformaldehyde. The distal metaphysis was analyzed with a Skyscan 1072 μ-CT instrument (Skyscan, Antwerp, Belgium). Regions of interest (ROIs) in the distal portion of each femur started from the proximal border of the growth plate (0.0–2.5 mm from the growth plate border). Image acquisition was performed at 100 kV and 98 μA, with a 0.9° rotation between frames. The two-dimensional images were used to generate three-dimensional reconstructions to obtain quantitative data with the 3D Creator software supplied with the instrument. Nomenclature and abbreviations of 3D μ-CT parameters follow the recommendations of the American Society for Bone and Mineral Research [20].

2.5. Biochemical analyses

Mice ($n = 10$/group) were euthanized at week 6 of treatment, and blood was removed by cardiac puncture. Calciotropic hormones were measured using specific kits for parathyroid hormone (PTH) (Immunotopics Inc. San Clemente, CA, USA) and 25(OH)D (ImmunoDiagnostic Systems Ltd., UK). Serum calcium and glucose were quantified using customary biochemical analysis. Type 1 procollagen amino-terminal-propeptide (P1NP) and C-telopeptide (CTx) were measured by enzyme immunoassay (EIA) (Immunodiagnostics Systems Limited, Boldon, UK) according to the manufacturer's instructions.

2.6. Histological and histomorphometry analysis of skin and bone

The details of these methods were described previously [21,22]. Detection of alkaline phosphatase and TRAP activity in bone was carried out as previously described [22]. Naphtol-AS-TR (Sigma-Aldrich, Australia) was used as substrate for both enzymes; Fast Blue BB salt (Sigma-Aldrich, Australia) was used as a coupler for alkaline phosphatase. Von Kossa staining was used to perform histomorphometry of marrow fat.

For dynamic histomorphometry, tetracycline labeling of bones was achieved through the intraperitoneal injection of demeclocycline (20 mg/kg) (Sigma Chemicals, St. Louis, MO, USA) to the three groups at 5 and 2 days before sacrifice. One femur from each animal in each group was removed at the time of euthanasia, fixed in 70% ethanol, dehydrated, and embedded undecalcified in methylmethacrylate (J-T Baker, Phillipsburg, NJ, USA). At 50 μm intervals, longitudinal sections of 5 and 8 μm thick were cut using a polycut-E microtome (Reichert-Jung Leica, Heerbrugg, Switzerland), placed on gelatin-coated glass slides, deplastified and stained with Goldner's trichrome. Histomorphometry was performed with a semi-automatic image analyzing system combining a microscope equipped with a camera lucida and digitizing tablet linked to a computer using the OsteoMeasure Software (Osteometrics Inc., Decatur, GA, USA). Nomenclature and abbreviations of histomorphometry parameters follow the recommendations of the American Society for Bone and Mineral Research [23].

In addition to standard hematoxylin/eosin (H/E) staining, immunohistochemistry (IHC) of tibiae and skin sections was performed. Bone sections were incubated overnight at 4 °C with a goat polyclonal antibody IgG against RANKL (Santacruz Biotechnology Inc. Santa Cruz CA, USA). Bone and skin sections were incubated overnight at 4 °C with a goat polyclonal antibody IgG against PR domain containing 16 (PRDM16) (Cat. # AF6295, R&D Systems). Primary antibody was detected by incubation with an anti-goat IgG secondary antibody conjugated with HRP (1:300 in BSA 1%, Sigma-Aldrich, St. Louis, MO, USA). Antibody complexes were visualized with DAB, a 3, 3-diaminobenzine solution containing hydrogen peroxide (ImmunoCruz™ mouse ABC Staining System, Santacruz Biotechnology Inc. Santa Cruz CA, USA) and then counterstained in 1% hematoxylin. Images were captured at two different magnifications (10× and 40×) using a Nikon Eclipse E100 microscope (Nikon Instruments Inc., Melville, NY, USA). Brightness and contrast adjustments were performed in Photoshop (Adobe). Levels of RANKL and PRDM16 expression were quantified as percentage of bone marrow surface using the Bioquant Image Analysis Software.

2.7. Fat quantification

For marrow fat analysis, the right femur was cleaned of soft tissue, fixed for 36 h in 4% paraformaldehyde, rinsed thoroughly in PBS, decalcified in 10% EDTA and processed for paraffin embedding. Serial 4-μm sections cut on a modified Leica RM 2155 rotary microtome (Leica Microsystems, Richmond Hill, Ontario, Canada). Percentage of marrow fat content was calculated as fat volume/total volume (FV/TV) using Von Kossa stained sections as previously described [21,22]. For subcutaneous fat, percentage of fat was calculated as fat volume/total volume (FV/TV) using hematoxylin/eosin stained sections.

2.8. Osteoclast culture and treatment

RAW264.7 cells were maintained in suspension culture in non-coated Petri dishes (Grenier Bio-One, Monroe, NC, USA) in high glucose DMEM supplemented with 10% heat-inactivated fetal bovine serum, 100 μg/ml streptomycin, 100 U/ml penicillin, in a humidified atmosphere of 5% CO2 at 37 °C. For experiments, cells were plated in a 48-well plate at 4×10^3 cells/well and treated with RANKL (30 ng/ml) (Santa Cruz, SC-4618) with or without cerulenin for 3 or 4 days. Bone marrow derived osteoclasts were generated by sacrificing 6–12-week-old C57/BL6 mice and flushing the tibiae and femurs with α-MEM to obtain bone marrow cells. After removing erythrocytes with ACK Lysing Buffer (LONZA, #10-548E), cells were cultured in α-MEM containing heat-inactivated fetal bovine serum, 100 μg/ml streptomycin, 100 U/ml penicillin and 20 ng/ml macrophage colony-stimulating factor (M-CSF) (R&D systems, #416-ML) overnight. Adherent cells were discarded, and non-adherent cells were transferred to a 24-well plate at 5×10^5 cells/well and cultured in the presence of M-CSF (30 g/ml) and RANKL (40 ng/ml) with or without cerulenin for 5 days. To confirm the presence of osteoclasts, cells were stained for TRAP according to the manufacturer's instructions (Sigma-Aldrich, #387A-1KT). TRAP positive multinuclear cells (> 3 nuclei) were counted utilizing Tablet Draw software and NIH ImageJ. For pit assay, RAW264.7 cells (0.025×10^6/well) were cultured on Osteo Assay Plate (Corning #3987) for 7 days with RANKL (30 ng/ml) with or without various concentrations of cerulenin. Osteoclasts formed at day 4. To measure the pit areas, at day 7 the cells were removed by treating the plate with 5% sodium hypochlorite for 5 min. Plates were washed with water and dried. Pictures were taken under a microscope at 20× magnification. The resorbed areas were then quantified by using ImageJ software. The results are expressed as the total areas of the resorption.

2.9. Statistical analysis

The mice sample size for each experiment was calculated based on alpha error of 0.2 and a beta error of 0.05 with a significant power > 90% to detect a 10% absolute difference in the parameters of bone formation (BMD, Ob number, bone biomarkers and dynamic histomorphometry) and 10% reduction in fat volume. Differences between groups were determined by using Levene's test for homogeneity of variances and unpaired *t*-test for equality of means for histomorphometry measurements. All other variables were compared using one- and two-way analysis of variance (ANOVA). In all experiments, a value of $p < 0.05$ was considered significant.

3. Results

3.1. Inhibition of FAS decreases weight and fat mass in OVX C57BL/6 mice

Cerulenin has been reported as an inducer of weight loss [24]. Initially, we examined the impact of 6 weeks of treatment with cerulenin (30 mg/kg/d, subcutaneous, three times per week) in 36-week old CER-OVX mice as compared to either VEH-OVX or SHAM operated controls. Both groups showed similar water and food intake throughout the study. Whereas the VEH-OVX mice exhibited a significant increase in body weight (~−21 ± 3%), CER-OVX mice showed significantly lower weight as compared to both SHAM and VEH-OVX controls ($p < 0.01$, Fig. 1B). Subsequently, we measured serum concentrations of triglycerides as an indicator of FAS inactivation, which decreases triglyceride release from the liver [25]. In agreement with previous reports [26], VEH-OVX mice showed a significant reduction in serum triglycerides as compared to SHAM controls ($p < 0.01$, Fig. 1B). Cerulenin treatment potentiated this effect indicating that FAS activity was reduced in the CER-OVX group. On the other hand, as FAS is regulated by glucose intake [27], we tested the effect of FAS inhibition on glucose levels of treated and untreated mice. Serum glucose was not affected as a result of cerulenin treatment in this model (Table 2).

To determine whether the effect on weight and fat is associated with a reduction in leptin, a hormone that has been associated with the regulation of bone turnover in this model [28], we quantified serum concentrations of leptin in the three groups. We found that leptin levels were significantly increased in the VEH-OVX group and still increased, but to a lesser degree in the CER-OVX mice compared to the SHAM controls (Fig. 1B).

Subsequently, to better understand the mechanism of action of cerulenin in this model, we tested changes in the transcription and translation levels of the major adipogenic gene peroxisome proliferator activator receptor gamma-2 (PPARγ-2) (Fig. 1C), and gene expression of the adipogenic genes CCAAT/enhancer binding protein alpha (C/EBPα) and adipocyte protein 2 (aP2) (Fig. 1C) in OVX mice group with and without cerulenin treatment. We found no difference in gene and protein expression in CER-OVX mice as compared to the VEH-OVX controls.

We then tested the effect of FAS inhibition on both subcutaneous and marrow fat. The CER-OVX mice exhibited significant decreases in subcutaneous fat as compared to both SHAM and VEH-OVX controls (Fig. 1D $p < 0.001$). This reduction in subcutaneous fat of the CER-OVX mice was concomitant with significantly lower levels of marrow fat volume/total volume (FV/TV) (Fig. 1E, $p < 0.001$). Adipocyte parameters such as size (AD size, μm^2) and number (AD#/mm^2) reflected high lipid content in the VEH-OVX group as compared with SHAM. On the other hand, these parameters were significantly decreased in CER-OVX mice as compared with VEH-OVX and were equivalent to those observed in SHAM (Fig. 1E).

In addition, the *ex vivo* adipogenic potential of bone marrow stromal cells (BMSC) to differentiate into adipocytes was markedly reduced as evidenced by significantly lower number of differentiated adipocytes in the CER-OVX group along with a noticeable change in their phenotype in culture with a minimum of adipocytes showing a normal ellipsoidal shape and fat droplets and the majority showing an unusual form and scarce cytoplasmic fat (Fig. 1F, $p < 0.01$). These morphological changes in the differentiated adipocytes *ex vivo* were supported by ORO quantification ($p < 0.01$), which was significantly lower in BMSC obtained from cerulenin-treated mice (Fig. 1F).

To expand the understanding of cerulenin action on cells within the adipogenic lineage and to identify a potential effect of this treatment on local energy metabolism, we investigated changes in the presence of a brown fat transcription factor (PRDM16) in bone marrow (Fig. 1G) and subcutaneous (Fig. 1H) fat by using IHC. We observed PRDM16 to be significantly decreased in marrow cells and subcutaneous fat from VEH-OVX mice as compared with SHAM whereas its expression in CER-OVX samples was significantly higher than VEH-OVX (Fig. 1G and H, $p < 0.001$).

Table 2
Circulating concentrations of glucose, Ca and calciotropic hormones parathyroid hormone (PTH), 25(OH)-vitamin D [25(OH)D] in nine-month-old OVX C57BL/6 mice treated with either cerulenin (CER-OVX) or vehicle (VEH-OVX).

Assay	SHAM	VEH-OVX	CER-OVX	P value
	N = 8	N = 8	N = 8	
Glucose (mg/dl)	104 ± 12	108 ± 14	96 ± 15	*NS*
Calcium (mg/dl)	8.3 ± 0.2	8.5 ± 0.4	8.1 ± 0.2	*NS*
25(OH)D (nmol/l)	54 ± 12	60 ± 16	52 ± 14	*NS*
PTH (pg/ml)	36 ± 6	38 ± 5	34 ± 5	*NS*

3.2. Inhibition of FAS reverses bone loss and induces bone formation thus correcting the osteoporotic phenotype in OVX C57BL/6 mice

We assessed qualitative and quantitative microarchitecture data of sagittal and posterior sections of distal femurs using μCT and Von Kossa staining (Fig. 2A). There was a significant increase in bone volume/total volume (BV/TV) in the CER-OVX group as compared to the VEH-OVX group ($p < 0.01$), reaching the same levels observed in the SHAM controls (Fig. 2A). Cerulenin treatment resulted in similar gains in other bone parameters, including structure model index (SMI), trabecular thickness (Tb.Th.), cortical thickness (Ct.Th.) and trabecular number (Tb.N.) ($p < 0.01$). Subsequently, we performed dynamic histomorphometry by measuring the mineral apposition rate (MAR) of both cortical and trabecular bone using fluorochrome staining (Fig. 2B). Treatment with cerulenin induced a significant increase in MAR in both trabecular and cortical bone as compared to both SHAM and VEH-OVX groups ($p < 0.001$) (Fig. 2B). Taken together, our morphometric analysis indicates that FAS inhibition induces high levels of bone formation thereby rescuing OVX mice from their osteoporotic phenotype.

3.3. Inhibition of FAS increases bone mass by inducing osteoblastogenesis and decreasing osteoclastogenesis in vivo

The apparent anabolic effect of FAS inhibition on bone was further examined by quantifying the number of bone forming cells (osteoblasts) and bone resorbing cells (osteoclasts) *in situ* and measuring circulating concentrations of markers of their activity. After normalization to the bone surface, a significant increase in osteoblast number was seen in CER-OVX mice (Fig. 3A) compared to the VEH-OVX group ($p < 0.01$). The increase in osteoblast number could be associated with an increase in serum P1NP (Fig. 3A), which is used as a biomarker for bone formation in the clinical setting.

In striking contrast to the effect observed in the osteoblast lineage, cerulenin induced a significant decrease in osteoclast number, as evidenced by TRAP staining and lower serum CTx (Fig. 3B) in the CER-OVX group relative to the VEH-OVX group. These data suggested an uncoupling of bone formation from resorption by favoring osteoblast bone formation while decreasing osteoclast number and activity, an effect that is independent of serum levels of calciotropic hormones (Table 2).

We further explored this uncoupling effect by testing the bone marrow levels of gene and protein expression of receptor activator of nuclear factor kappa-B ligand (RANKL), an important mediator of cell coupling and communication between osteoblasts and osteoclasts, which has been associated with high levels of marrow fat and lipotoxicity [10]. As expected, OVX resulted in higher levels of gene and protein expression of RANKL (Fig. 3C), whereas treatment with cerulenin significantly reduced RANKL gene and protein expression compared to the VEH-OVX group. This suggests that cerulenin may uncouple bone formation and bone resorption in part by inhibiting

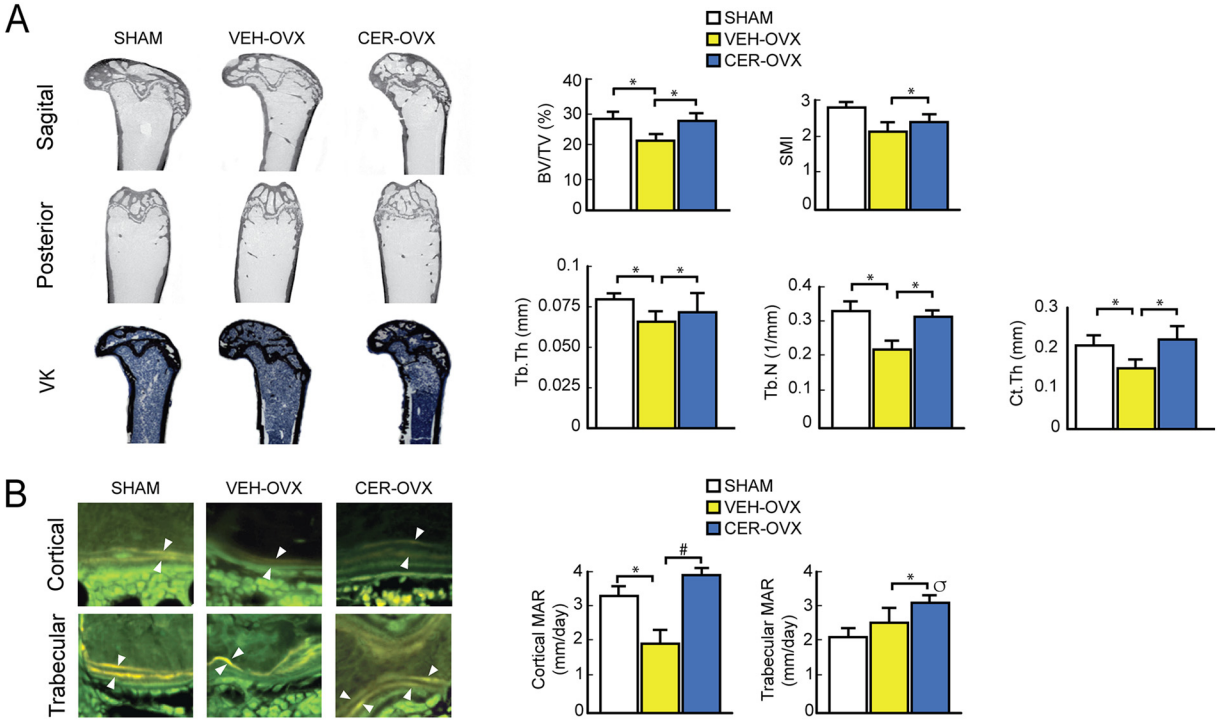

Fig. 2. Effect of cerulenin on bone microarchitecture. (A) μ-CT and von Kossa (left, lower panels) analysis of bone structure. Histomorphometry parameters included bone volume/total volume (BV/TV), structure model index (SMI), trabecular thickness (Tb.Th.), cortical thickness (Ct.Th.) and trabecular number (Tb.N.). (B) Dynamic histomorphometry shows changes in mineral apposition rate (MAR) in both cortical and trabecular bone in the three mouse groups. Magnification 40×. Values are mean ± SD, *$p < 0.05$, #$p < 0.001$, σ $p < 0.05$ between the SHAM and the VEH-OVX and CER-OVX groups (n = 10/group).

expression of RANKL thus affecting the communication between osteoblasts and osteoclasts.

We then tested whether cerulenin treatment exerts a direct effect on bone cells that could lead to these structural and biochemical changes. We have previously reported that cerulenin has no effect on osteoblast function and survival *in vitro* [5]. We assessed whether treatment with cerulenin affects osteoclast differentiation, function and survival *in vitro*. As shown in Fig. 4A–B, treatment with cerulenin had no effect on osteoclast number and differentiation in culture. In addition, no effect was found on osteoclast survival. Furthermore, pit experiments showed that resorption was not affected upon cerulenin treatment in osteoclasts derived from RAW264.7 cells (Fig. 4C). This evidence suggests that the anabolic and uncoupling effects of cerulenin are not due to a direct effect on bone cells but to an indirect effect mediated through the inhibition of FAS and to a reduction in levels of marrow fat.

3.4. Inhibition of FAS favors ex vivo mineralization and stimulates transcription factors of bone formation

Subsequently we compared the *ex vivo* osteoblastic differentiation potential of BMSC obtained from CER-OVX and VEH-OVX groups. The final stage of differentiation was determined by testing mineralization and differentiation using alizarin red and alkaline phosphatase staining respectively. Alkaline phosphatase production was no different between the groups (Fig. 4D). In contrast, alizarin red staining indicated that calcium deposition, characteristic of matrix formation at the end of differentiation, was two-fold increased in the CER-OVX group compared to the VEH-OVX mice ($p < 0.01$). There was no difference between the SHAM and VEH-OVX groups (Fig. 4D).

Finally, to characterize the stimulatory effect of cerulenin on bone formation *in vivo*, we assessed gene and protein expression of the osteogenic factors RUNX2, OPN, OCN and BSP in BMSC obtained from VEH-OVX and CER-OVX groups. Cerulenin treatment induced significantly higher levels of mRNA of OPN (six-fold), OCN and BSP ($p < 0.001$), but no changes in RUNX2 expression, compared to expression in VEH-OVX samples (Fig. 4E). RUNX2 and OCN levels of protein expression in VEH-OVX samples remained stable, whereas OPN was significantly increased ($p < 0.01$) in the CER-OVX samples (Fig. 4E).

4. Discussion

Using an animal model that combines increased levels of marrow fat and significant bone loss, we tested our hypothesis that inhibition of FAS *in vivo* would enhance bone formation and rescue OVX mice from osteoporosis. Our results indicate that FAS inhibition increases bone formation and modulates bone resorption not only by decreasing fat levels and their end-products but also by facilitating osteoblastic activity and mineralization, inducing a higher number of mature osteoblasts, and inhibiting the communication between osteoblast and osteoclasts *via* RANKL. By inhibiting FAS we have decreased fatty acid secretion, reduced body weight and fat mass, increased bone formation, modulated high levels of bone resorption, and overall attenuated the deleterious effect that OVX has on bone in this model. Interestingly, all these effects were obtained by regulating fat mass and not by any apparent direct effects on bone cells in clear contrast with the mechanism of action of the current osteoporosis treatments.

Regarding the mechanisms that explain these effects, and in clear concordance with our previous *in vitro* studies [5], inhibition of FAS increased the expression of osteogenic transcription factors thus facilitating osteoblast function while also increasing mineralization. In addition, an important finding of this study was the higher levels of OPN expression observed in bone marrow from the cerulenin-treated animals. Since low levels of OPN would promote adipocyte differentiation [29], it is then expected that cerulenin-induced expression of OPN in OVX mice would restore a normal balance between adipogenesis and osteogenesis thus facilitating bone formation.

In addition, we propose that, as in our *in vitro* models, cerulenin

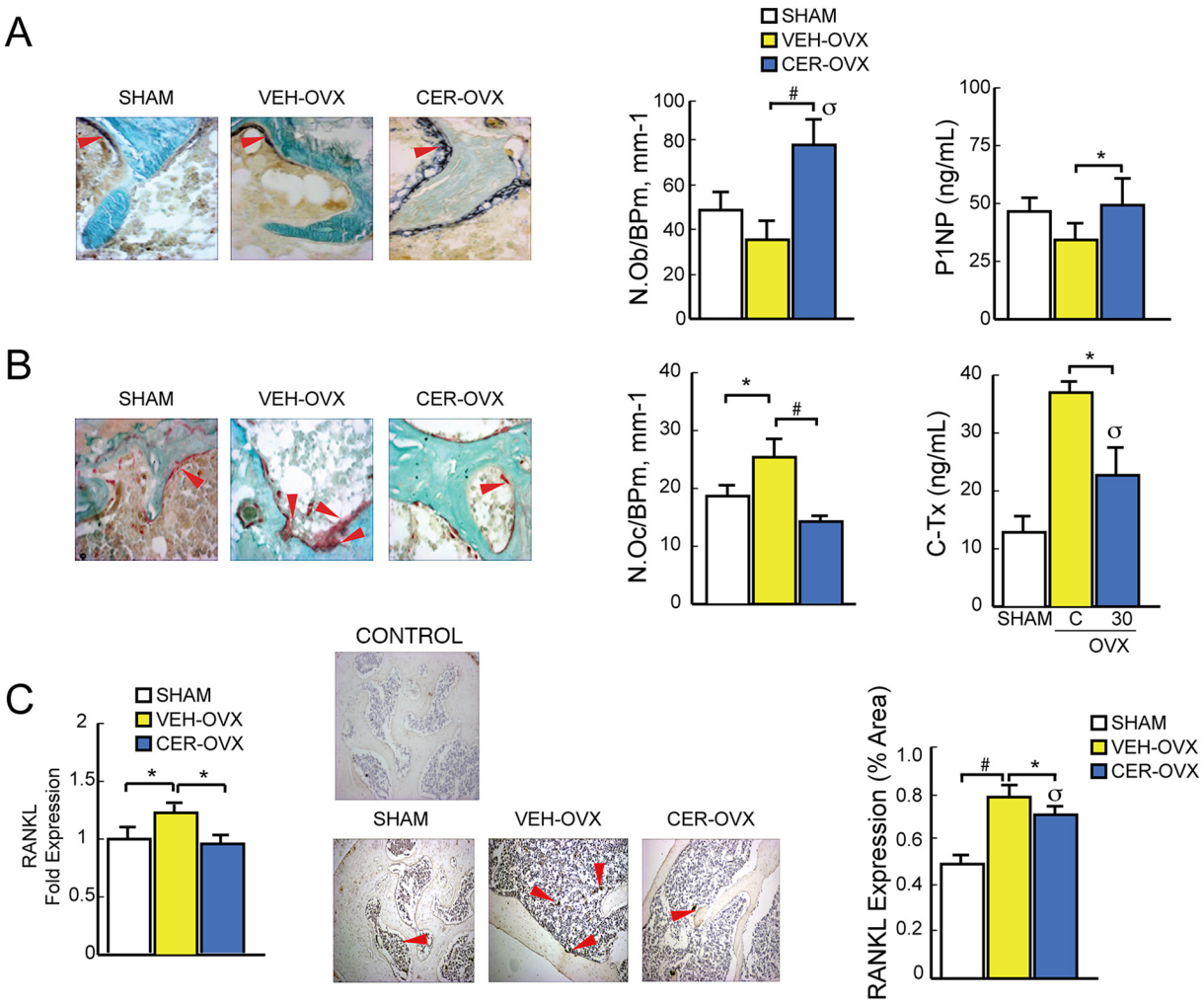

Fig. 3. Effect of cerulenin on bone turnover. (A) A significant increase in the number of ALP expressing cells (osteoblasts) was observed in mice treated with cerulenin compared with the other mice groups, which was concomitant with higher serum concentrations of P1NP. In contrast, staining of bone with TRAP (B) showed a significant reduction in the number of cells stained in red corresponding to osteoclasts (OC) (arrows) the cerulenin-treated OVX mice with lower serum concentration of CTx. Micrographs are representative of those from ten different mice of each treatment group. Arrows indicate representative cells/areas in each section, and magnification was 20×. Values are mean ± SD, $^{*}p < 0.05$, $\#p < 0.001$, $\sigma\ p < 0.05$ between the SHAM and the VEH-OVX and CER-OVX groups. (C) RANKL expression in the bone marrow was quantified by RT-PCR and IHC (magnification 10×). (For interpretation of the references to colour in this figure legend, the reader is referred to the web version of this article.)

helped to maintain high levels of mature osteoblasts in the marrow milieu as a natural response to lower levels of marrow fat together with a reduction in adipocyte-secreted lipotoxic products. This local effect could be independent of systemic fat-secreted regulators of the neuroendocrine access that affect bone metabolism such as leptin [30], which was significantly reduced by cerulenin in OVX animals. Indeed, the effect of cerulenin in bone cells could be also exerted through other additional mechanisms, which were not explored in this study. Cerulenin also appears to be an inhibitor of sterol synthesis and is an HMG-CoA synthase inhibitor, which would mimic the osteogenic effect of statins [31] and could partially explain the anabolic effect of cerulenin in this mouse model.

To further explore the effect of cerulenin on energy metabolism in this model, we quantified the expression of PRDM16, a major surface marker of brown adipose tissue (BAT), within the subcutaneous and bone marrow tissues. BAT could be increased in response to changes in energy metabolism [32]. Additionally, it has been demonstrated that BAT is required for osteoblastogenesis [4,33]. In agreement with a previous study [34], OVX induced a significant reduction in marrow and subcutaneous BAT. This effect was reversed by treatment with cerulenin, which was more significant in the marrow fat, thus suggesting that additionally to the osteogenic effect of cerulenin, the increasing levels of BAT could exert a co-adjuvant effect on promoting osteoblastogenesis and bone formation. Regarding the direct effect of cerulenin on adipocytes, our previous *in vitro* data demonstrated that this effect is limited to inhibiting their capacity to produce fatty acids without affecting their differentiation and survival [5]. We also tested whether inhibition of FAS was associated with lipodystrophy or potential redistribution of fat. Analysis of subcutaneous muscle and liver did not show differences in fat volumes between cerulenin-treated and control mice (data no shown). However, a comprehensive investigation of ectopic fat infiltration in other organs was not performed.

Previously, we have tested the hypothesis that fat loss is bone gain using a mouse model of osteoporosis [35]. We reported that fat inhibition could have an anabolic effect on male C57BL/6 mice through the inhibition of peroxisomal proliferator-activated receptor gamma (PPARγ); an essential transcription factor for adipogenesis. Pharmacological inhibition of PPARγ in 9-month-old OVX C57BL/6 mice induced high levels of osteoblastogenesis and bone formation concomitant with decreased marrow adiposity and *ex vivo* adipogenesis. In the present study, and considering that adipocytes are still required for multiple metabolic functions, we did not target adipocyte differentiation as a

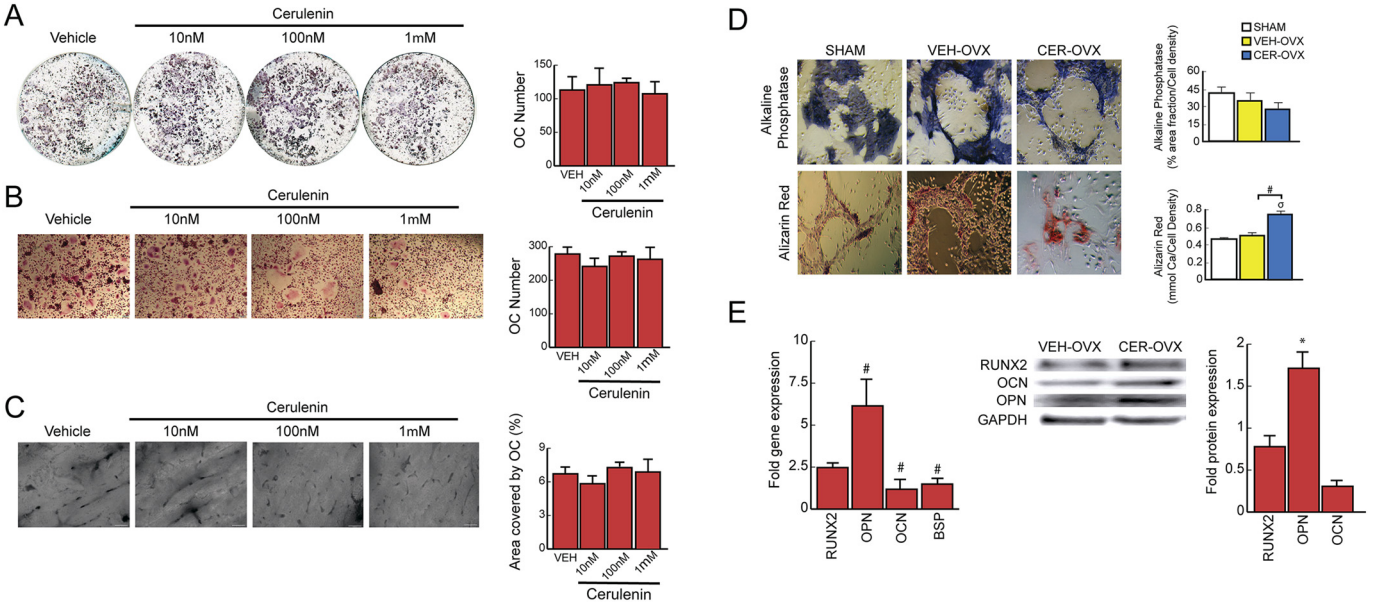

Fig. 4. Effect of cerulenin on osteoclast and osteoblast differentiation and function. Osteoclasts were generated from RAW264.7 cells (A) and bone marrow cells (B) as described in the methods, and differentiation was unaffected by increasing doses of cerulenin. TRAP staining was performed and quantitation of multi-nucleated (≥3 nuclei) TRAP stained cells was assessed (A, B). Results are representative of three separate experiments. Values in the charts are mean ± SD, $*p < 0.05$, $\#p < 0.001$, σ significant difference between the SHAM and the VEH-OVX and CER-OVX groups. (C) Pit resorption experiments in osteoclasts formed from RAW264.7 cells, expressed as area covered (%) by osteoclasts after cerulenin treatment. VEH = RANKL (30 ng/ml). Magnification 20×.
Ex vivo culture of BMSC under osteogenic conditions showed no changes in extracellular alkaline phosphatase (D, upper panels) quantification but did exhibit significantly higher levels of mineralization (D, lower panels), expressed as molar equivalent of calcium present in the alizarin red-calcium complex. Magnification 40×. (E) Gene and protein expression of osteogenic markers in bone marrow obtained from VEH-OVX and CER-OVX mice. Results are representative of three separate experiments. Fold expression represents CER-OVX relative to VEH-OVX samples. Values are mean ± SD, $*p < 0.05$, $\#p < 0.001$.

whole but their capacity to produce FAS and thus to secrete potentially toxic fatty acids in the bone marrow milieu, which is a completely novel therapeutic target in osteoporosis.

We therefore propose that FAS inhibition, particularly treatment with cerulenin or its analogues, could become a therapeutic approach to osteoporosis in the future. The therapeutic window of cerulenin is narrow due to its potential toxicity and side effects such as severe anorexia and weight loss. These side effects have been associated with the increased activation of fatty acid oxidation (FAO) [36], which is only induced by high doses such as 60 mg/kg daily for 7 days [18] or 80 mg/kg daily for 7 days [15]. In contrast, lower and intermittent doses, such as the one used in this and other studies [37,38], induced a significant fall in body weight and triglyceride levels without having any major side effects on the energy metabolism. Therefore, for the purposes of this study, we selected a low dose that was calculated in accordance with previous *in vitro* [5] and *in vivo* [25,38] experiments. Other natural and synthetic analogues of cerulenin have been tested based on their ability to block fatty acid production and adipocyte differentiation [39,40]. Their effectiveness on preventing bone loss in this or other animal models of osteoporosis will be a subject of future studies.

Taken together, our data support our hypothesis that inhibition of FAS could represent an anabolic approach to the treatment of osteoporosis. We propose that FAS inhibition generates a “friendly” environment within the bone marrow milieu that, associated with other potential mechanisms such as inhibition of HMG-CoA synthase, increases osteoblast number while facilitating osteoblast activity and mineralization and concomitantly preventing bone resorption. Although this approach should be tested in other classical models of osteoporosis, ours is the first evidence demonstrating that FAS inhibition is feasible without apparent side effects. In conclusion, we have demonstrated that marrow fat could constitute an effective therapeutic target for osteoporosis that deserves further exploration in the near future.

Disclosure

All authors state that they have no conflicts of interest.

Acknowledgments

This study was supported by grants from the Australian National Health and Medical Research Council (NHMRC 632767), the Australian Institute for Musculoskeletal Science (AIMSS), the Nepean Medical Research Foundation, the U.S. Department of Veterans Affairs (Merit Review), and the Indian Trail Foundation. Support was also received from the Miami VAHS GRECC and Research Service. M. Hernandez and M. Rodriguez provided technical assistance. The authors would like to thank Professor David Handelsman for his continuous support to this study.

Authors' roles

Study design: GD, SB, CV. Study conduct: GD and CV. Data collection: GD, CV, SB, AAS, MK, MP, DM and BRT. Data analysis: GD, SB, AAS, DM and BRT. Data interpretation: GD, SB, AAS, DM and BRT. Drafting manuscript: GD, CV SB, AAS, DM and BRT. Revising manuscript content: GD, CV, SB, AAS, DM and BRT. Approving final version of manuscript: All authors. SB takes responsibility for the integrity of the data analysis.

References

[1] D.M. Black, C.J. Rosen, Clinical practice. Postmenopausal osteoporosis, N. Engl. J. Med. 374 (3) (2016) 254–262.
[2] S. Khosla, L.C. Hofbauer, Osteoporosis treatment: recent developments and ongoing challenges, Lancet Diabetes Endocrinol. 5 (11) (2017) 898–907.
[3] C.J. Rosen, M.L. Bouxsein, Mechanisms of disease: is osteoporosis the obesity of bone? Nat. Clin. Pract. Rheumatol. 2 (1) (2006) 35–43.
[4] L. Singh, S. Tyagi, D. Myers, G. Duque, Good, bad, or ugly: the biological roles of bone marrow fat, Curr. Osteoporos. Rep. 16 (2) (2018) 130–137.

[5] A. Elbaz, X. Wu, D. Rivas, J.M. Gimble, G. Duque, Inhibition of fatty acid biosynthesis prevents adipocyte lipotoxicity on human osteoblasts in vitro, J. Cell. Mol. Med. 14 (4) (2010) 982–991.
[6] K. Gunaratnam, C. Vidal, J.M. Gimble, G. Duque, Mechanisms of palmitate-induced lipotoxicity in human osteoblasts, Endocrinology 155 (1) (2014) 108–116.
[7] K. Gunaratnam, C. Vidal, R. Boadle, C. Thekkedam, G. Duque, Mechanisms of palmitate-induced cell death in human osteoblasts, Biol. Open 2 (12) (2013) 1382–1389.
[8] Stedman's, Lipotoxicity, Stedman's Medical Dictionary, 28th ed., Lippincott Williams & Wilkins, Philadelphia, 2005, p. 2100.
[9] A. Sepe, T. Tchkonia, T. Thomou, M. Zamboni, J.L. Kirkland, Aging and regional differences in fat cell progenitors - a mini-review, Gerontology 57 (1) (2011) 66–75.
[10] S.R. Oh, O.J. Sul, Y.Y. Kim, H.J. Kim, R. Yu, J.H. Suh, H.S. Choi, Saturated fatty acids enhance osteoclast survival, J. Lipid Res. 51 (5) (2010) 892–899.
[11] M.C. Kuhn, H.S. Willenberg, M. Schott, C. Papewalis, U. Stumpf, S. Flohe, W.A. Scherbaum, S. Schinner, Adipocyte-secreted factors increase osteoblast proliferation and the OPG/RANKL ratio to influence osteoclast formation, Mol. Cell. Endocrinol. 349 (2) (2012) 180–188.
[12] T.H. Ambrosi, T.J. Schulz, The emerging role of bone marrow adipose tissue in bone health and dysfunction, J. Mol. Med. 95 (12) (2017) 1291–1301.
[13] B. Lecka-Czernik, S. Baroi, L.A. Stechschulte, A.S. Chougule, Marrow fat-a new target to treat bone diseases? Curr. Osteoporos. Rep. 16 (2) (2018) 123–129.
[14] S. Verma, J.H. Rajaratnam, J. Denton, J.A. Hoyland, R.J. Byers, Adipocytic proportion of bone marrow is inversely related to bone formation in osteoporosis, J. Clin. Pathol. 55 (9) (2002) 693–698.
[15] E.S. Pizer, F.J. Chrest, J.A. DiGiuseppe, W.F. Han, Pharmacological inhibitors of mammalian fatty acid synthase suppress DNA replication and induce apoptosis in tumor cell lines, Cancer Res. 58 (20) (1998) 4611–4615.
[16] D.H. Fu, Z.L. Liu, J.S. Liu, Y. Luo, Y. Shu, S.H. Huang, Z.M. Han, Transepithelial transport of Cerulenin across Caco-2 cell monolayers, Eur. J. Drug Metab. Pharmacokinet. 34 (2) (2009) 67–72.
[17] Y.M. Kim, H.T. Shin, Y.H. Seo, H.O. Byun, S.H. Yoon, I.K. Lee, D.H. Hyun, H.Y. Chung, G. Yoon, Sterol regulatory element-binding protein (SREBP)-1-mediated lipogenesis is involved in cell senescence, J. Biol. Chem. 285 (38) (2010) 29069–29077.
[18] R. Akter, D. Rivas, G. Geneau, H. Drissi, G. Duque, Effect of lamin A/C knockdown on osteoblast differentiation and function, J. Bone Miner. Res. 24 (2) (2009) 283–293.
[19] M.W. Pfaffl, Relative expression software tool (REST(C)) for group-wise comparison and statistical analysis of relative expression results in real-time PCR, Nucleic Acids Res. 30 (9) (2002) e36.
[20] M.L. Bouxsein, S.K. Boyd, B.A. Christiansen, R.E. Guldberg, K.J. Jepsen, R. Muller, Guidelines for assessment of bone microstructure in rodents using micro-computed tomography, J. Bone Miner. Res. 25 (7) (2010) 1468–1486.
[21] W. Li, L.S. Yeo, C. Vidal, T. McCorquodale, M. Herrmann, D. Fatkin, G. Duque, Decreased bone formation and osteopenia in lamin a/c-deficient mice, PLoS One 6 (4) (2011) e19313.
[22] G. Duque, W. Li, L.S. Yeo, C. Vidal, D. Fatkin, Attenuated anabolic response to exercise in lamin A/C haploinsufficient mice, Bone 49 (3) (2011) 412–418.
[23] D.W. Dempster, J.E. Compston, M.K. Drezner, F.H. Glorieux, J.A. Kanis, H. Malluche, P.J. Meunier, S.M. Ott, R.R. Recker, A.M. Parfitt, Standardized nomenclature, symbols, and units for bone histomorphometry: a 2012 update of the report of the ASBMR Histomorphometry Nomenclature Committee, J. Bone Miner. Res. 28 (1) (2013) 2–17.
[24] C.V. Mobbs, H. Makimura, Block the FAS, lose the fat, Nat. Med. 8 (4) (2002) 335–336.
[25] S. Murata, K. Yanagisawa, K. Fukunaga, T. Oda, A. Kobayashi, R. Sasaki, N. Ohkohchi, Fatty acid synthase inhibitor cerulenin suppresses liver metastasis of colon cancer in mice, Cancer Sci. 101 (8) (2010) 1861–1865.
[26] A. Ludgero-Correia Jr., M.B. Aguila, C.A. Mandarim-de-Lacerda, T.S. Faria, Effects of high-fat diet on plasma lipids, adiposity, and inflammatory markers in ovariectomized C57BL/6 mice, Nutrition 28 (3) (2012) 316–323.
[27] M. Wu, S.B. Singh, J. Wang, C.C. Chung, G. Salituro, B.V. Karanam, S.H. Lee, M. Powles, K.P. Ellsworth, M.E. Lassman, C. Miller, R.W. Myers, M.R. Tota, B.B. Zhang, C. Li, Antidiabetic and antisteatotic effects of the selective fatty acid synthase (FAS) inhibitor platensimycin in mouse models of diabetes, PNAS 108 (13) (2011) 5378–5383.
[28] J.J. Cao, L. Sun, H. Gao, Diet-induced obesity alters bone remodeling leading to decreased femoral trabecular bone mass in mice, Ann. N. Y. Acad. Sci. 1192 (2010) 292–297.
[29] Q. Chen, P. Shou, L. Zhang, C. Xu, C. Zheng, Y. Han, W. Li, Y. Huang, X. Zhang, C. Shao, A.I. Roberts, A.B. Rabson, G. Ren, Y. Zhang, Y. Wang, D.T. Denhardt, Y. Shi, An osteopontin-integrin interaction plays a critical role in directing adipogenesis and osteogenesis by mesenchymal stem cells, Stem Cells 32 (2014) 327–337.
[30] R.T. Turner, S.P. Kalra, C.P. Wong, K.A. Philbrick, L.B. Lindenmaier, S. Boghossian, U.T. Iwaniec, Peripheral leptin regulates bone formation, J. Bone Miner. Res. 28 (1) (2013) 22–34.
[31] F. Ruan, Q. Zheng, J. Wang, Mechanisms of bone anabolism regulated by statins, Biosci. Rep. 32 (6) (2012) 511–519.
[32] K. Ikeda, P. Maretich, S. Kajimura, The common and distinct features of brown and beige adipocytes, Trends Endocrinol. Metab. 29 (3) (Mar 2018) 191–200.
[33] A. Krings, S. Rahman, S. Huang, Y. Lu, P.J. Czernik, B. Lecka-Czernik, Bone marrow fat has brown adipose tissue characteristics, which are attenuated with aging and diabetes, Bone 50 (2) (2012) 546–552.
[34] A. Nadal-Casellas, A.M. Proenza, I. Llado, M. Gianotti, Effects of ovariectomy and 17-beta estradiol replacement on rat brown adipose tissue mitochondrial function, Steroids 76 (10 − 11) (2011) 1051–1056.
[35] G. Duque, W. Li, C. Vidal, S. Bermeo, D. Rivas, J. Henderson, Pharmacological inhibition of PPARγ increases osteoblastogenesis and bone mass in male C57BL/6 mice, J. Bone Miner. Res. 28 (2013) 639–648.
[36] Y.J. Jin, S.Z. Li, Z.S. Zhao, J.J. An, R.Y. Kim, Y.M. Kim, J.H. Baik, S.K. Lim, Carnitine palmitoyltransferase-1 (CPT-1) activity stimulation by cerulenin via sympathetic nervous system activation overrides cerulenin's peripheral effect, Endocrinology 145 (7) (2004) 3197–3204.
[37] B. Schmid, J.F. Rippmann, M. Tadayyon, B.S. Hamilton, Inhibition of fatty acid synthase prevents preadipocyte differentiation, Biochem. Biophys. Res. Commun. 328 (4) (2005) 1073–1082.
[38] Z.L. Liu, G. Wang, Y. Shu, P.A. Zou, Y. Zhou, Q.S. Yin, Enhanced antitumor activity of epirubicin combined with cerulenin in osteosarcoma, Mol. Med. Rep. 5 (2) (2012) 326–330.
[39] S.R. Smith, K.S. Stenlof, F.L. Greenway, J. McHutchison, S.M. Schwartz, V.B. Dev, E.S. Berk, R. Kapikian, Orlistat 60 mg reduces visceral adipose tissue: a 24-week randomized, placebo-controlled, multicenter trial, Obesity 19 (9) (2011) 1796–1803.
[40] T.S. Ho, Y.P. Ho, W.Y. Wong, L. Chi-Ming Chiu, Y.S. Wong, V. Eng-Choon Ooi, Fatty acid synthase inhibitors cerulenin and C75 retard growth and induce caspase-dependent apoptosis in human melanoma A-375 cells, Biomed. Pharmacother. 61 (9) (2007) 578–587.